Microchemical Journal 227 (2026) 118653

Contents lists available at ScienceDirect

Microchemical Journal

journal homepage: www.elsevier.com/locate/microc

Nanomaterial-enhanced voltammetric sensor for concurrent monitoring of aprepitant and apixaban in plasma toward precision medicine and in pharmaceutical analysis

Rasha Th. El-Eryan [a], Mona S. Elshahed [a], Dalia Mohamed [a], Azza A. Ashour [a,*], Heba T. Elbalkiny [b]

[a] Pharmaceutical Analytical Chemistry Department, Faculty of Pharmacy, Capial Universiy (previously Helwan University), 11795 Cairo, Egypt
[b] Analytical Chemistry Department, Faculty of Pharmacy, October University for Modern Sciences and Arts (MSA), 11787 6th October City, Egypt

ARTICLE INFO

Keywords:
Precision medicine
Aprepitant
Apixaban
ZnO NPs
Carbon dots
MWCNTs

ABSTRACT

The growing demand for precision medicine has driven the development of nanomaterial-modified electrodes for applications in this field. This work reports novel voltammetric platforms based on functionalized carbon paste electrodes (CPEs) with engineered nanomaterials for the concurrent determination of aprepitant (APR) and apixaban (APX) in human plasma, as well as the first voltammetric assay for APR in pharmaceutical capsules. Monitoring both drugs is clinically relevant because APR may inhibit APX metabolism, increasing bleeding risk during coadministration. For simultaneous plasma analysis, a CPE was modified with 2% zinc oxide nanoparticles (ZnO NPs) and 1% carbon dots (CDs) synthesized from pepper seeds, a sustainable green precursor. This nanocomposite-modified sensor achieved linear ranges of 0.28–1.31 μM (0.15–0.70 μg/mL) for APR and 0.02–1.09 μM (0.01–0.50 μg/mL) for APX. For individual determination of APR in capsules, a CPE incorporating 1% multi-walled carbon nanotubes (MWCNTs) and 1% CDs provided a linear range of 0.19–2.06 μM (0.10–1.10 μg/mL). All proposed methods were validated according to international guidelines. Furthermore, the greenness of the analytical procedures was systematically evaluated, confirming their environmental compatibility and alignment with sustainable chemistry principles. The developed sensors offer a promising step toward a precision medicine strategy for therapeutic drug monitoring and risk assessment of drug-drug interactions, with potential for integration into portable diagnostic devices. In addition, they demonstrate valuable applicability in pharmaceutical quality control laboratories.

1. Introduction

Aprepitant (APR) (**Fig. S1**) is an antiemetic drug used to prevent nausea and vomiting associated with emetogenic chemotherapy and postoperative. The drug is not used for patients who already have nausea or vomiting [1]. APR acts by penetrating the blood-brain barrier and antagonizing the neutrokine neurotransmitters in the brain, which cause nausea and vomiting [2]. The maximum plasma concentration of the drug in blood was declared to be 1.4 μg/mL with T_{max} 4 h, and the plasma protein binding is 97%, after administering a 125 mg dose [3]. The drug is eliminated mainly after metabolism by liver enzymes; any drug that acts as a substrate to hepatic enzymes may affect the therapeutic efficiency of APR. Also, Patients with severe hepatic impairment may need frequent monitoring of APR and adjustment of its dose to obtain an effective response [4].

Apixaban (APX) (**Fig. S1**) is an anticoagulant agent used for the prevention and treatment of venous thromboembolism in various cases, the prophylaxis of thromboembolism stroke, and the treatment of cases with pulmonary embolism [5]. This drug works by inhibiting clotting factor Xa; thus, it takes a longer timeframe for blood to form clots [6]. The maximum plasma concentrations of the drug in blood were declared to be 105 and 176 ng/mL with T_{max} between 2 and 4 h after administering 5 and 10 mg tablets, respectively, and the plasma protein binding is 87% [7]. Patients with cancer are susceptible to venous thromboembolism, which has been announced as the most frequently reported cause of mortality unrelated to cancer progression. Furthermore, this population is susceptible to significant bleeding; in the context of their situation, cancer-associated thrombosis guidelines recommended the

* Corresponding author.
E-mail addresses: azza.abdellateef@pharm.helwan.edu.eg, azza.abdellateef@pharm.capu.edu.eg (A.A. Ashour).

https://doi.org/10.1016/j.microc.2026.118653
Received 2 April 2026; Received in revised form 20 May 2026; Accepted 6 June 2026
Available online 11 June 2026

use of low molecular weight heparin and non-vitamin K antagonist anticoagulant (like APX) for their situation [8]. A moderate interaction between APR and APX was addressed in some patients treated with those drugs simultaneously, as APR is a known Cytochrome P450 3A4 inhibitor, which is responsible for the metabolism of APX [9]. This interaction ultimately leads to an increase in the plasma concentration of APX and the risk of bleeding. Personalized dosing of APX would have a substantial impact on avoiding major bleeding in those cancer patients. Currently, clinical management mainly depends on monitoring patients for bleeding manifestations after the interaction has already occurred. However, this approach may not prevent adverse effects at an early stage. Therefore, our approach supports appropriate dose adjustment before serious bleeding complications develop. In addition, aprepitant undergoes extensive hepatic metabolism through CYP3A4, making its plasma concentration susceptible to alteration by many co-administered anticancer drugs. Monitoring aprepitant is clinically important because it plays a key role in preventing chemotherapy-induced nausea and vomiting, thereby improving patients' quality of life and treatment adherence. Therefore, simultaneous monitoring of both drugs could enhance the safety and therapeutic effectiveness of the combined regimen.

Precision medicine is an innovative approach that came to the fore to offer the most suitable drug regimen to the right patient with real-time decisions. One approach to achieve that is by monitoring the patient's response to the drug regimen, which could be observed as the circulating blood concentration of the drug [10]. The current challenge is to provide a precision medicine platform for monitoring the circulating drugs in the bloodstream without time-consuming procedures and with simple steps, ultimately motivating healthcare providers to create a tailored regimen.

To our knowledge, few analytical approaches have been developed for the determination of APR, including a voltametric method [11], spectrophotometric methods [12–14], and chromatographic methods [15–19]. Several methods were validated for the determination of APX, including spectrophotometric methods [20–24], spectrofluorometric method [25], chromatographic methods [26–34], and two electrochemical methods were developed for individual determination of APX [35,36]. The large equipment and low sensitivity of spectrophotometers, as well as difficulties in operations and maintenance of chromatographic equipment, curtail their utility in precision medicine applications. To date, no method has been reported for the simultaneous determination of APR and APX in plasma, and there is no voltammetric method available for the routine analysis of APR in pharmaceutical dosage forms.

The appeal of voltammetric sensors lies in their potential to provide sensitive, rapid, reliable, and easily fabricated portable sensors for the determination of versatile drugs in various matrices [37]. The advantages of various nanoparticles have widened the avenues for their use as modifiers in carbon paste electrodes. The active surface area of the multiwall carbon nanotubes (MWCNTs) and zinc oxide nanoparticles (ZnO NPs) provides a catalytic activity in the voltammetric determinations. The conductivity of the electrode is enhanced by the incorporation of such nano-materials as a result of increasing the electronic stream, besides the porous structure of the MWCNTs, which increases the surface-to-volume ratio and subsequently the active surface area of the working electrode [38–41]. The allure of modified carbon paste with carbon dots (CDs) has gained much interest. Using organic waste as a feedstock for the preparation of CDs is a crucial step toward developing analytical methods with environmental compatibility. The incorporation of such nanocarbonaceous materials enhances the sensitivity of the method owing to an increase in the conductivity of the electrode and improves the selectivity, which is attributed to the active surface area with various functional groups [42,43]. Incorporation of different nanoparticles into the CPE matrix creates a synergistic effect that significantly enhances the electrochemical performance of the sensor [37–41]. The pivotal end goal of this study is to provide a reliable and sustainable method for determining APR in marketed capsules and to design sensor useful in precision medicine by providing a simultaneous determination of APR and APX in human plasma.

2. Experimental

2.1. Materials and reagents

APR authentic powder was supplied by the Egyptian Drug Authority with a purity of 99.12%. APX authentic powder was supplied by Mina Pharm with a purity of 99.36%. Bell peppers, Emend® (125 and 80 mg capsules), and Apixatrack (5 mg film-coated tablets) were purchased from the local market. Human plasma was obtained from Nasr institute, Egypt. MWCNT (more than 95% carbon) with an outer diameter of 6–9 nm and a length of 5 mm, ZnO NPs (particle size less than 50 nm, 99.5% trace metals basis), zeolite, graphite powder (particle size ranging between 1 and 2 μm), paraffin oil, sodium hydroxide, phosphoric acid, glacial acetic acid, HPLC-grade methanol, ethyl acetate, and hexane were all obtained from Sigma-Aldrich, Germany. Potassium ferrocyanide and boric acid were obtained from Piochem, Egypt. Sodium carbonate and sodium bicarbonate were obtainer from El-Nasr company. Britton–Robinson buffer solutions (BRS) in the pH range of 2.0 to 10.0 were used as supporting electrolytes. The buffer solutions were prepared by mixing boric acid, acetic acid, and phosphoric acid at a concentration of 0.4 M. The resulting solution was then diluted to obtain a 0.04 M buffer after adjusting the pH using 0.1 M NaOH [44]. Carbonate buffer at pH 9.8 was prepared by mixing 0.1 M $NaCO_3$ and 0.1 M $NaHCO_3$ [19].

2.2. Instrumentation

A Metrohm voltmeter equipped with a 50 cm^3 electrochemical cell connected to a three-electrode system was utilized for the voltammetric measurements. A platinum wire served as the auxiliary electrode, while an Ag/AgCl reference electrode filled with 3.0 M KCl was used as the reference electrode. Data acquisition and analysis were carried out using the Viva software (version 2.0). pH measurements were performed using a Hanna pH meter (HI 2211) coupled with a glass electrode. A domestic microwave (LG, 900 W) was used for the preparation of CDs. Additional instrumentation included a lyophilizer (Thermo Fisher), a centrifuge (CENCE), and a sonicator (POWERSONIC 410), all of which were employed in the developed analytical procedures. A Thermo Fisher Scientific vortex mixer was used.

2.3. Preparation of environmentally compatible CDs

CDs were prepared as previously described and fully characterized by our team [45]. A 5 g sample of bell pepper seeds was weighed and steeped in 5 mL of distilled water, followed by microwave irradiation for approximately 15 min until a dark brown coloration was observed, indicating carbonization. For the extraction of CDs, the resulting charred seeds were soaked in 15 mL of double-distilled water. The slurry was first filtered using standard filter paper, followed by a second filtration through a 0.22 μm syringe filter to remove fine particulates. The resulting CDs-containing filtrate was then frozen and subsequently subjected to lyophilization to obtain a dry CDs powder. The powdered CDs were then incorporated into the formulation of the carbon paste electrode (CPE) as a nanostructured modifier.

2.4. Preparation of the working carbon paste electrodes (CPE)

Throughout all prepared electrodes, 0.50 g of graphite powder was used. For the preparation of bare CPE, 0.50 g of graphite was poured into a porcelain dish, and approximately 0.2 mL of paraffin oil was added and blended thoroughly with the powder until an evenly mixed paste with the desired consistency was formed. For the preparation of different modified CPEs, the equivalent weight of the modifier powder was subtracted from the amount of graphite powder, so that the total sum of the

used powder remained equivalent to 0.50 g. The calculated amount of the modifier was blended thoroughly with the corresponding amount of graphite powder, and then nearly 0.2 mL of paraffin oil was added and mixed well until a homogeneous paste with the desired consistency was obtained. Each prepared paste was packed individually into the electrode body, which was connected to the three-compartment cell of the voltmeter [46,47].

2.5. Preparation of standard stock and working solutions

Standard stock solutions of 1.00 mg/mL APR and APX were prepared by accurately dissolving 0.01 g of each authentic powder to 10.00 mL of methanol. Standard working solutions were then prepared by transferring 1.00 mL of the stock solution into a 10-mL volumetric flask and adjusting the volume with the same diluent, resulting in a working solution with a concentration of 0.10 mg/mL. The prepared working solution was subsequently used for the construction of the calibration curve.

2.6. Preparation of APR capsule solutions

The contents of Emend® capsules (one 125 mg and two 80 mg capsules in each strip) were combined, an amount equivalent to 0.01 g of APR was accurately weighed and transferred into a 10-mL volumetric flask. The volume was completed to the mark with methanol, and the flask was sonicated for 20 min to ensure complete extraction. This solution was designated as the capsule stock solution. The capsule working solution was then prepared following the same procedure described for the standard working solution in ***Section II.E***.

2.7. Preparation of plasma solutions

Plasma stock solution and four concentration levels; lower limit of quantitation (LLOQ) (0.28 and 0.02 μM for APR and APX, respectively), low-quality control sample (LQC) (0.56 and 0.06 μM for APR and APX, respectively), medium-quality control sample (MQC) (0.84 and 0.44 μM for APR and APX, respectively), and high-quality control sample (HQC) (1.12 and 0.87 μM for APR and APX, respectively), and plasma stock solution were prepared by adding appropriate aliquots from the standard working solutions and adjusting the volume to 5.0 mL with thawed plasma at ambient temperature. The spiked plasma solutions were vortex-mixed for 30 s to ensure thorough mixing.

Subsequently, a liquid-liquid extraction was performed. 1 mL of carbonate buffer (pH 9.8) was added to 4.0 mL of the spiked plasma. The drugs were then extracted with 8.0 mL of a solvent mixture composed of ethyl acetate and hexane in a 70:30 (*v*/v) ratio, added in successive portions [27]. Each addition was followed by vortex mixing for 3 min, after which the mixture was centrifuged at 10,000 rpm for 5 min. The resulting organic phase was carefully separated and evaporated to dryness under controlled conditions. The dried residue was then reconstituted in 1.0 mL of methanol, which was used for the construction of the calibration curve.

2.8. Construction of the calibration curve

To construct the calibration curve for the individual determination of APR, different aliquots from the working solution of APR were added to 10 mL of BRS (pH 10.0) in the volumetric cell to cover the linearity range of 0.19–2.06 μM. A 1% MWCNTs/1% CDs/CPE was used as the working electrode.

To construct the calibration curves for the simultaneous determination of APR and APX, different aliquots were taken from the prepared spiked human plasma to cover the linearity ranges of 0.28–1.91 μM for APR and 0.02–1.09 μM for APX. BRS at pH 4.0 was used, and a 2% ZnO/1% CDs/CPE electrode was employed as the optimized working electrode. The calibration curves were constructed by plotting the peak current (I_P) against the molar concentration of the studied.

3. Results and discussion

3.1. Effect of pH

Cyclic voltammetry (CV) is a powerful tool for investigating the electrochemical reactivity of the studied species using bare CPE. BRS, spanning a pH range of 2.0–11.0, was used in this study, with each drug present at a concentration of 3.00 μg/mL. Fig. 1a illustrates the CVs for APR, demonstrating the presence of two oxidation peaks at pH 5 and above. At lower pH values up to 4, only one oxidation peak is observed (the leftmost one). The maximum peak current was recorded with the left peak at pH 10. For APX (Fig. 1b), a single oxidation peak is apparent in the anodic scan. This peak is distinctly observed at both acidic and slightly alkaline pH values but disappears entirely at pH values above 8. The highest peak current was obtained at pH 5, with peak current at pH 4 coming next. The cathodic scan for both drugs lacks any reduction peaks, confirming that the oxidation process is irreversible. The potentials of the peaks shifted toward less positive values with increasing pH, indicating that the oxidation mechanism for both drugs is pH-dependent. This also suggests that a deprotonation step is involved in the oxidation mechanism [48]. The Nernst equation describes the relation between the peak potential and the change in pH:

$$E_p = -(0.0592\ y/n)\ pH + k$$

E_p is the peak potential, **y** represents the number of protons involved in the oxidation mechanism, and **n** denotes the number of electrons involved in the oxidation process (Fig. 1 **insets**). The slope values were found to be 0.0758 and 0.0793 for the left and right peaks of APR, respectively, and 0.0196 for APX. These values suggest that the number of protons involved in the oxidation mechanism of APR for both peaks is almost equal to the number of electrons, whereas the number of protons is fewer than the number of electrons in the case of APX.

For individual determination of APR, pH 10.0 was found to be the optimum value. For simultaneous determination of both drugs, we found that the optimum pH is 4.0, because at higher pH values the right peak of APR interferes with the oxidation peak of APX, impeding their simultaneous quantitative determination.

3.2. Electrode modifications

To enhance the electrochemical sensitivity and analytical performance of CPE, various nanomaterials (MWCNTs, ZnO, and CDs) and zeolite were incorporated into the electrode matrix, as depicted in Fig. 2. Among the tested modifiers, 1% MWCNTs and 1% CDs exhibited superior individual performance for APR detection, and their co-integration led to a pronounced synergistic effect, resulting in approximately a twofold increase in peak current relative to the bare CPE at pH 10. Furthermore, the peak potential (E_p) of APR shifted by 2 mV toward less positive values, indicating enhanced electron transfer kinetics and reduced anodic overpotential [48].

Upon investigating the modified electrode at pH 4, we found that the best response for APR was obtained using 1% CDs, followed by 1% MWCNTs, 2%CDs, then 1% ZnO, and finally 2% ZnO, each used individually. While for APX, it was found that 1% CDs and 2% ZnO gave the highest response for its oxidation peak. For simultaneous determination of APR and APX at pH 4, and to obtain the highest sensitivity for APX so we can obtain a reliable quantitative determination of its concentration in plasma, a binary modification strategy employing 2% ZnO and 1% CDs was adopted. This nanocomposite-modified CPE exhibited a synergistic enhancement in peak currents for both analytes, with nearly twofold increases in signal intensity relative to the unmodified CPE. Additionally, both APR and APX oxidation peaks displayed negative shifts in E_p, suggestive of more favorable redox kinetics and decreased activation energy for electron transfer.

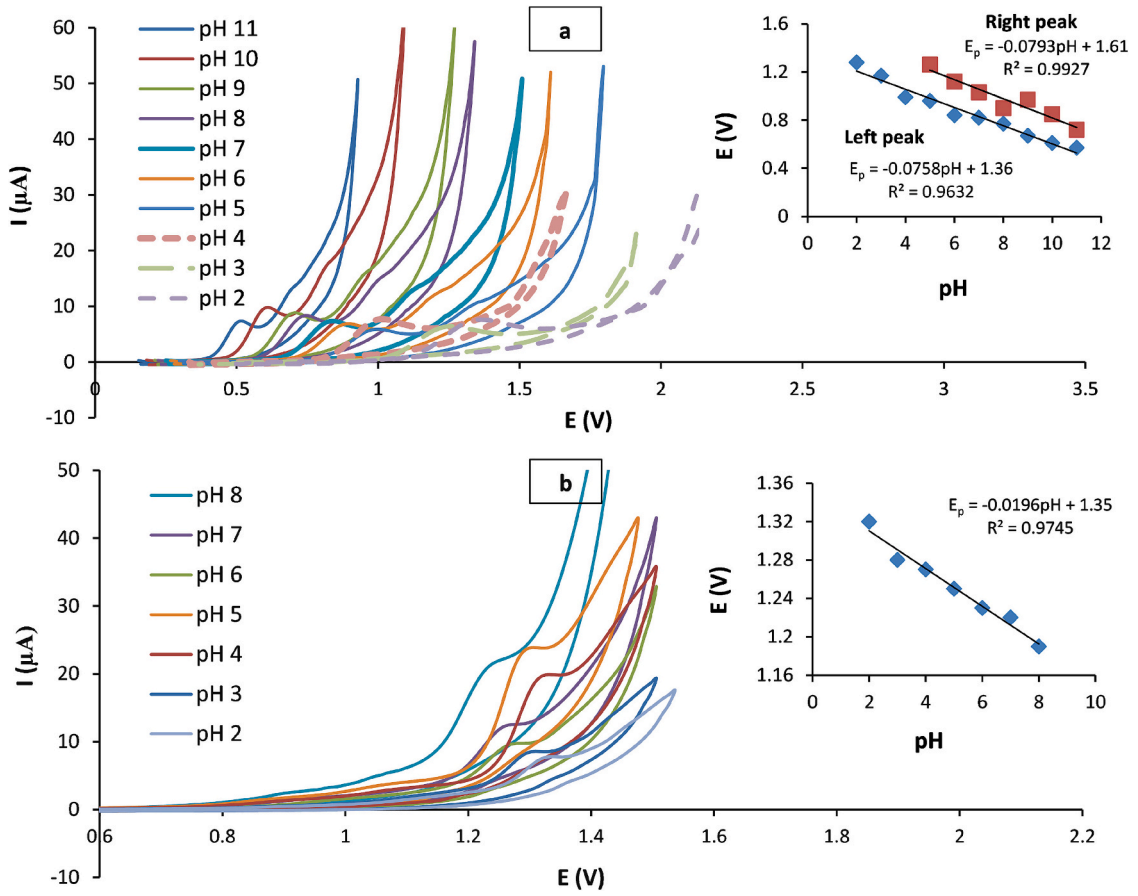

Fig. 1. Effect of pH using bare CPE on the voltammetric response of 3 µg/mL APR in a pH range from 2.0 to 11.0 (a), and the voltammetric response of 3.00 µg/mL APX in a pH range from 2.0 to 8.0 (b). Inset: plots of the peak potential (E_P) against the corresponding pH.

The enhanced electrocatalytic performance of modified CPE is likely attributed to multiple molecular-level interactions. Both APR and APX are π-electron-rich compounds, facilitating π–π stacking interactions with the sp^2-hybridized domains of CDs. Moreover, the presence of nitrogen atoms in their molecular structures enables hydrogen bonding with oxygen-containing functional groups (e.g., –OH, –COOH) on the surface of CDs, promoting preconcentration and increased local analyte availability. The high surface area and rich surface functionality of CDs contribute to improved analyte adsorption and electron mediation, collectively enhancing the electrochemical signal [43]. Among the distinctive traits of ZnO nanoparticles when utilized for the modification of CPE, those particles exhibit affinity toward oxygen-containing compounds, which may also justify the enhanced response observed [41]. Besides tiny particle size, the porous structure of the MWCNTs increases the surface-to-volume ratio and subsequently the active surface area of the working electrode. The combined effect of ZnO, MWCNTs, and CDs thus provides complementary interaction pathways (electrostatic, hydrogen bonding, and π–π interactions), leading to improved sensitivity, enhanced electron transfer rates, and better resolution of the oxidation peaks [37–41].

3.3. The influence of scan rate on the electrochemical process

To investigate the electrochemical behavior of the studied drugs on the optimized electrodes, the Randles-Sevcik equation was employed [49]. The effect of scan rate in the range of 20–200 mV/s on the magnitude of the peak current was studied at BRS pH 10.0 using 1% MWCNTs/1%CDs/CPE as the working electrode for APR and at BRS pH 4.0 using 2%ZnO/1%CDs/CPE for simultaneous determination of both drugs. The best repeatability was obtained at a scan rate of 100 mV/s with both methods after three replicates; therefore, this scan rate was used in subsequent measurements. For the determination of APR (Fig. 3), it was observed that the peak current corresponding to APR increased upon increasing the scan rate, but the right peak was obvious from a scan rate of 100 mV/s; the absence of the oxidation peak at low scan rates points to the fact that this step follows a reasonably fast process [50]. By plotting log peak current (log I_p) against log scan rate (log υ), straight lines were obtained with slopes equal to 0.8975 and 0.5148 for the left and the right peaks, respectively, indicating that the oxidation of APR follows an adsorption-diffusion process. For the simultaneous determination of both drugs at pH 4.0 (Fig. 3), it was observed that the peak currents corresponding to APR and APX increased upon increasing the scan rate. By plotting log I_p against log υ, straight lines were obtained with slopes equal to 0.5642 and 0.4690 for APR (the left) and APX (the right peak), respectively, indicating that the oxidation of APR at pH 4.0 on 2%ZnO/1% CDs/CPE following adsorption-diffusion process, while the oxidation of APX at the same condition follows diffusion mechanism [49].

Laviron's equation is a helpful tool to explain the chemical reaction that occurs at the surface of the working electrode [51]:

$$E_p = E^0 + 2.303RT/\alpha nF\left[\log RTK^0/\alpha nF + \log \upsilon\right]$$

In this equation, **R** is the gas constant (8.314 *J* K/mol), **T** is the temperature (298 K), **α** is the coefficient of electron transfer, **n** is the number of electrons, **F** is the Faraday constant (96,485C/mol), and **υ** is the scan rate. For APR at pH 10.0 using 1%MWCNTs/1% CDs, by plotting the E_P against log υ, yielded two regression lines for left and right peaks with slopes equal to 0.0598 and 0.0658, respectively (Fig.3). This slope is equal to (0.0592/αn). As α is known to lie between zero to unity, it was estimated to be 0.7 for left and right peaks, respectively, to match

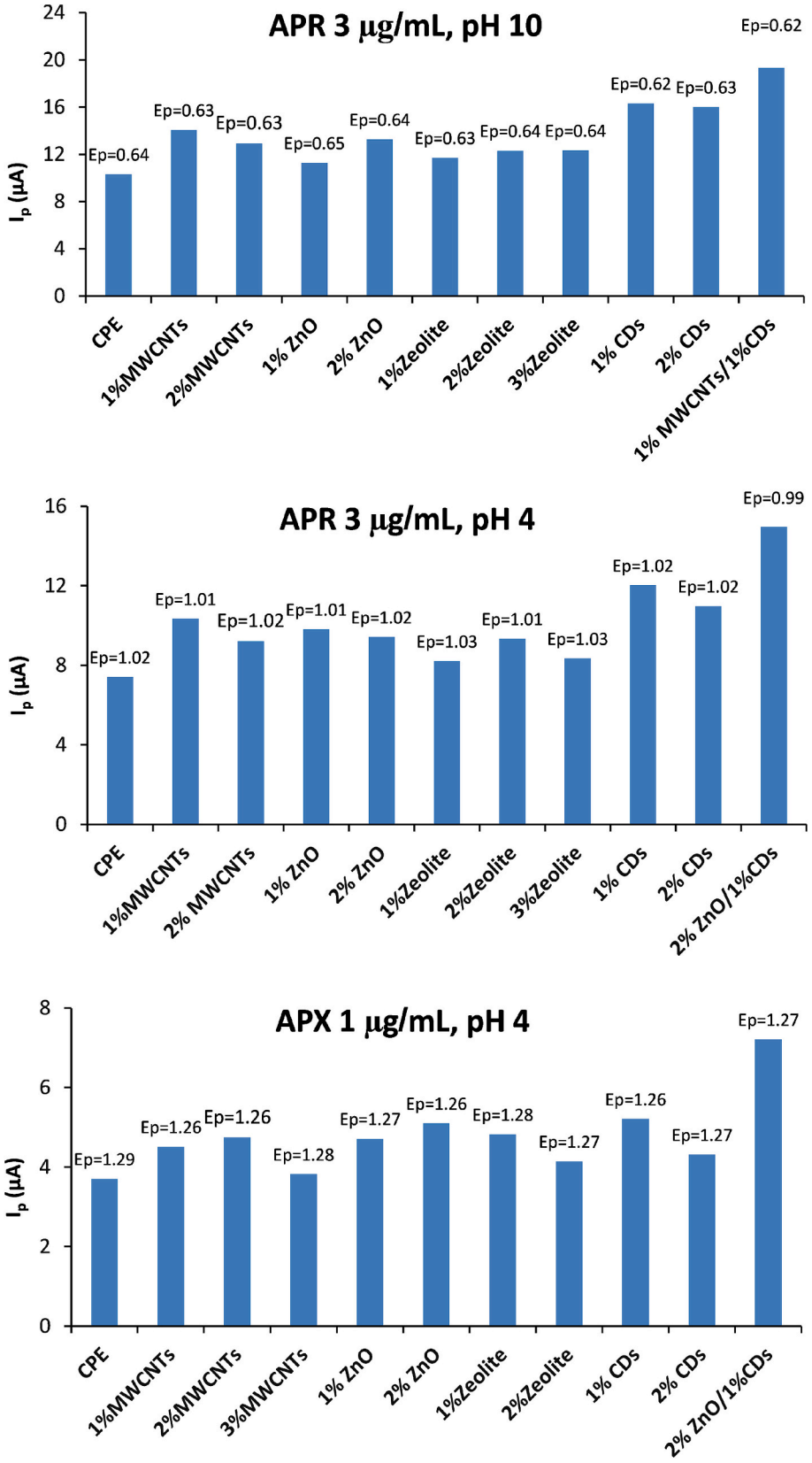

Fig. 2. Effect of different modifiers on the voltammetric response of 3 µg/mL APR alone using BRS at pH 10.0 and the voltammetric response of 3 µg/mL APR with 1 µg/mL APX simultaneously using BRS at pH 4.0.

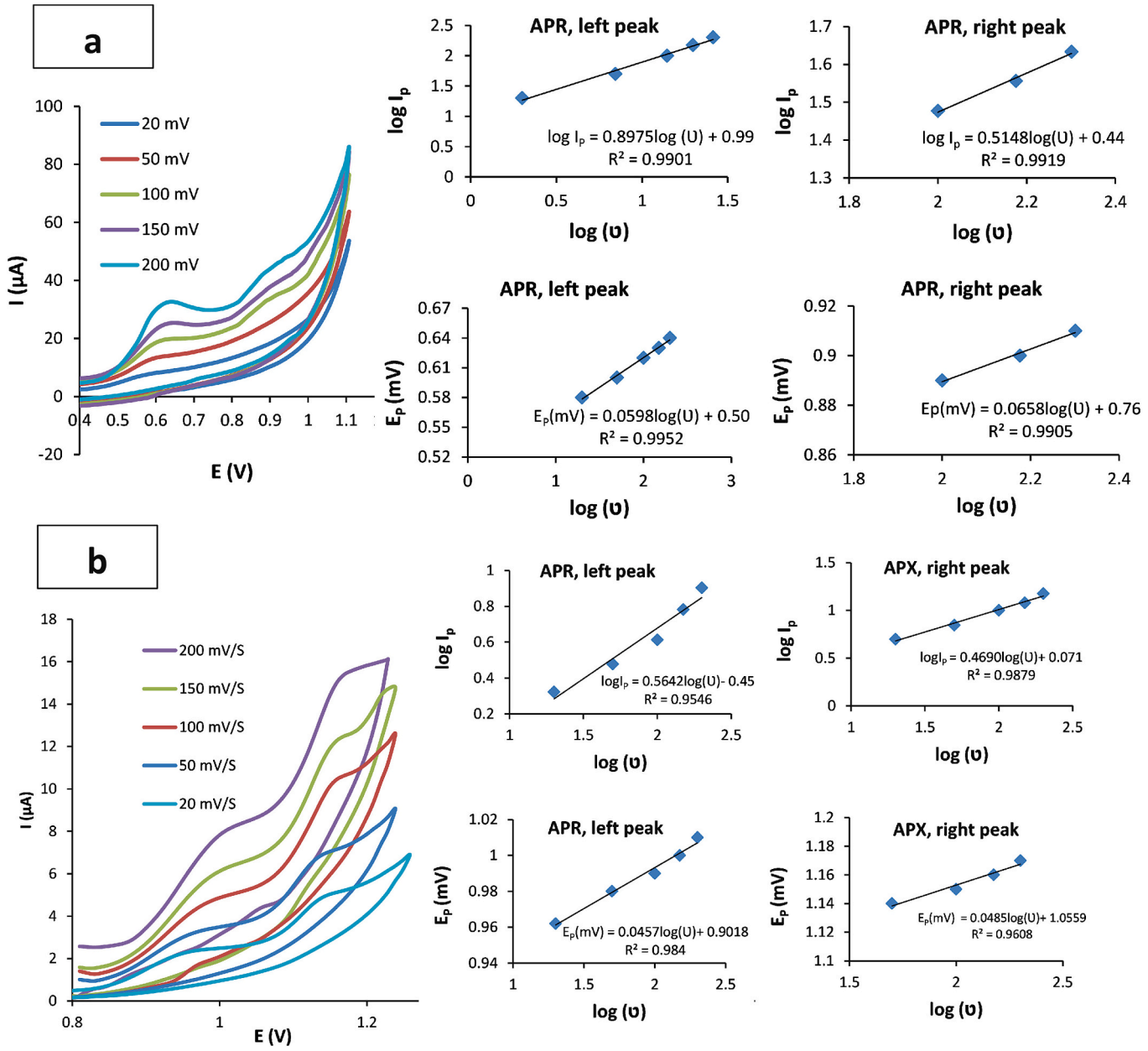

Fig. 3. Effect of different scan rates on the voltametric response of 3 µg/mL APR using 1%MWCNTs/1% CDs/CPE, BRS pH 10.0 (a) and on the simultaneous voltametric response of 3 µg/mL APR and 1 µg/mL APX using 2%ZnO/1%CDs/CPE, BRS at pH 4.0 (b).

the expected structure and the oxidation potential for the oxidation mechanism with one electron transfer for each peak.

The same graph was plotted for APR and APX, but at pH 4.0 using 2% ZnO/1%CDs/CPE. Two straight lines were plotted for both drugs, with slopes equivalent to 0.0457 and 0.0485 for APR and APX, respectively (Fig.3). The α values were estimated to be 0.9 and 0.6 for APR and APX, respectively, so the estimated number of electrons were found to be one and two electrons for APR and APX, respectively, which match the proposed mechanisms (Scheme 1) [48].

3.4. *Insight into the possible oxidation mechanisms*

In the triazolinone ring of APR, there are two NH groups. The NH group adjacent to the carbonyl and flanked by another nitrogen is more acidic due to resonance stabilization and electron-withdrawing effects. This site is likely deprotonated and oxidized even at low pH values, which explains the left oxidation peak, characterized by a loss of one electron and one proton with EC mechanism (Electron transfer followed by a Chemical reaction) (Scheme 1.**a**) [52]. The second NH group, which is less conjugated and hence less acidic, becomes fully protonated under acidic conditions (pH < 5). Its oxidation is suppressed at low pH, leading to the disappearance of the right oxidation peak, which also involves the loss of one electron and one proton with EC mechanism (Electron transfer followed by a Chemical reaction) (Scheme 1.**b**) [52]. Oxidation at the tertiary nitrogen of the morpholine ring is excluded as a contributing factor. Such oxidation would involve only electron transfer without associated proton loss, and would likely be pH-independent, contradicting the observed pH-dependent behavior [53]. This is consistent with prior electrochemical studies and supports the assignment of the redox processes to the triazolinone NH groups.

The single oxidation peak observed with APX is most likely attributed to the oxidation of the tertiary amide group, which occurs at a range of 1.2–1.5 V, while the oxidation of the primary amide occurs at a potential of 2.0 V and higher values [54]. The oxidation mechanism

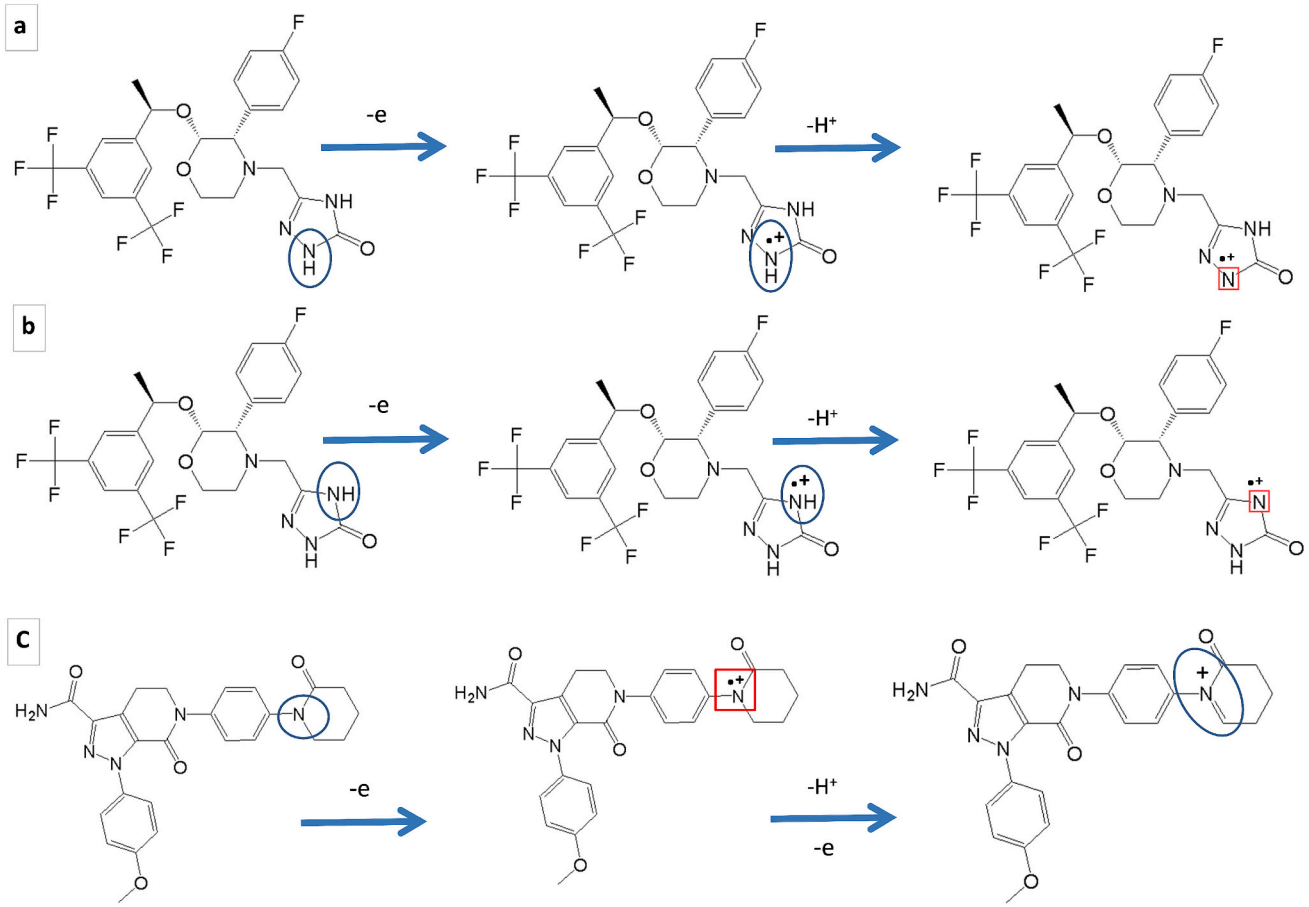

Scheme 1. The proposed oxidation mechanism for the left (a) and the right peaks (b) of APR and the single peak of APX (c)

involves the ECE mechanism (Electron transfer followed by a Chemical reaction, followed by Electron transfer) (Error! Reference source not found.**c**). Amides are relatively stable functional groups because of resonance stabilization between the carbonyl oxygen and the lone pair on the nitrogen.

$$R–CO–NR_2 \leftrightarrow R–C(\blacksquare O^{\blacksquare}) = NH_2^+$$

The bell-shaped oxidation profile, with a peak at pH 5.0, can be attributed to a balance of factors that promote both the formation and stabilization of the iminium cation product. At this mildly acidic pH, the nitrogen atom maintains sufficient electron density for initial oxidation, and the conditions are sufficient for α-carbon deprotonation [54], both essential for iminium formation.

At higher pH values, the resonance stabilization of the positive charge between nitrogen and carbon, which makes the carbocation more stable, is hindered. Also, the solvation of the iminium species through hydrogen bonding and ion–dipole interactions with water molecules is diminished. Therefore, pH 5.0 provides optimal conditions for both efficient electron transfer and effective stabilization of the oxidation product, resulting in the maximum observed current [55].

3.5. Effect of square wave voltammetry (SWV)

Screening the influence of SWV on the current signals of the studied drugs revealed that SWV produced higher response signals with both drugs compared to differential pulse voltammetry (DPV). Minimal interference from the non-faradaic capacitive current is involved in the SWV technique, while it yields a superior signal-to-noise ratio. For these reasons, this waveform technique maximizes sensitivity screening, making it particularly suitable for applications where maximum sensitivity is essential [56].

3.6. Screening the simultaneous determination of APR and APX

It is a crucial step to investigate whether any chemical interaction or cross-reactivity between the two studied drugs hinders their simultaneous determination. To this end, the concentration of one analyte was kept constant while varying the concentration of the other. As illustrated in **Fig. S2**, no interference was observed in the response of each drug.

3.7. Electrode characteristics

The scattering of the nanoparticles in the bulk of the graphite increases the surface area per unit of volume (surface area to volume ratio), thereby enhancing the electroactive surface area. Randles-Sevcik equation represents a successful tool to measure the electroactive surface of the working electrode [57]:

$$I_p = \left(2.96 \times 10^5\right).n^{3/2}.A.D^{1/2}.C.\upsilon^{1/2}$$

In this equation, the current response is represented as $\mathbf{I_P}$, the electrons involved in the redox reaction are given as **n**, whereas **A** is the electroactive surface area (cm^2), **D** is the symbol for the diffusion coefficients, for $K_4(Fe(CN)_6$ it is equivalent to 7.6×10^{-6} cm^2 s^{-1}, the concentration of the measured species (mol cm^{-3}) is expressed as **C**, and **υ** is the used scan rate (V s^{-1}). By using 20.0 mM $K_4Fe(CN)_6$, the electroactive surface area for the bare and the modified electrodes was measured in 0.1 M KCl using various scan rates. The peak currents were plotted against the square root of the scan rate, and from the slope of the regression line, **A** was computed. The modified electrodes with nanoparticles sprinkled exhibit higher currents compared to the bulk

graphite in the bare electrode. For the bare electrode, the electroactive surface area was found to be 0.05 cm^2, while for 1%MWCNTs/1%CDs and 2%ZnO/1%CDs they were 0.08 and 0.10 cm^2, respectively.

3.8. Validation of the proposed sensor

ICH and FDA were employed to verify the validation of the developed analytical method [58,59]. Two analytical curves were developed under different conditions for the individual determination of APR in capsule dosage form and the simultaneous determination of APR and APX in human plasma.

3.8.1. Validation of the proposed analytical method for the individual determination of APR in capsule dosage form

Individual determination of APR was performed using 1% MWCNTs/1% CDs/CPE at BRS pH 10.0 (Fig.4). The corresponding regression line was explicit as $I_p = 1.9457C + 0.46$, and the obtained linearity range was 0.19–2.06 μM. Limits of quantification (LOQ) and the detection (LOD) were obtained using the standard deviation of the intercept, which was multiplied by 10 for LOQ and 3.3 for LOD, and then the result was divided by the value of the slope of the analytical curve. The estimated LOQ and LOD were 0.15 and 0.04 μM, respectively. The accuracy of the studied concentrations was found to be 100.04 with SD 2.01. The repeatability and reproducibility of the method were validated using three different concentrations of APR; each concentration was determined in triplicate on the same day to validate the repeatability and on three different days to validate the reproducibility. As shown in Table 1, the average recovery in the case of repeatability was 100.05 with %RSD 1.41, whereas the obtained average recovery in the case of reproducibility was 100.56 with %RSD 1.54.

3.8.2. Validation of the proposed analytical method for the simultaneous determination of APR and APX in spiked human plasma

For the simultaneous determination of APR and APX in spiked plasma, 2%ZnO/1%CDs/CPE electrode was used in BRS at pH 4.0. The validation parameters were linearity range with limits of detection and quantitation, precision and accuracy, selectivity, carry-over effect, absolute recovery, matrix effect, different conditions for the stability, and dilution integrity; according to bio-validation guidelines of the FDA [59]. Four-level concentrations: lower limit of quantitation (LLOQ), low-quality control sample (LQC), which is equivalent to two or three times the LLOQ, medium-quality control sample (MQC), which represents the concentration corresponding to 40–60% of the linearity range, and finally high-quality control sample (HQC), which represents the concentration corresponding to 75–90% of the upper linearity range.

Table 1
Regression analysis and analytical validation for individual determination of APR in authentic powder.

Working electrode			1% MWCNTs/1% CDs/CPE
Linearity range			0.19–2.06 μM (0.10–1.10 μg/mL)
Coefficient of determination R^2			0.9988
Slope			1.9457
Intercept			0.46
LOQ			0.15 μM (0.08 μg/mL)
LOD			0.04 μM (0.02 μg/mL)
Accuracy	%Recovery		100.04
	±SD		2.01
Precision	Repeatabiliy	% Recovery	100.05
		%RSD	1.41
	Reprouducibility	% Recovery	100.56
		%RSD	1.54

The acceptance criteria were that the LLOQ did not deviate by more than 20% from the nominal concentration, and other concentrations did not deviate from the nominal concentrations by more than 15%.

3.8.2.1. Linearity range with limits of detection and quantitation. Human plasma was spiked with different aliquots to cover the linearity ranges 0.28–1.31 μM and 0.02–1.09 μM for APR and APX, respectively, with the corresponding regression equations $I_p = 1.7281C - 0.40$ with R^2 0.9970 and s $I_p = 0.4060C + 0.17$ with R^2 0.9996 for APR and APX, respectively, as shown in Fig. 5. The accepted criterion is that at least 75% of the calibration points fulfill the stated criteria. The limits of quantitation were 0.25 and 0.02 μM, and the limits of detection were 0.07 and 0.01 μM for APR and APX, respectively (Table 2). The obtained linearity range for APR was wider with higher sensitivity when it was determined individually, which is attributed to the competition between the analytes, besides the previously optimized condition of the working electrode.

3.8.2.2. Accuracy and precision. Accuracy and precision data were evaluated at four concentration levels. Accuracy was expressed as % recovery and precision as %RSD. QC concentrations were measured in six replicates on the same day (intraday validation), yielding accuracy values ranging from 97.31% to 101.31% for APR, and from 97.32% to 100.36% for APX. Precision ranged from 2.31% to 4.21% for APR and from 1.98% to 3.32% for APX. The same concentration levels were measured on three different days, each in six replicates (inter-day validation). The results showed accuracy values ranging from 97.12% to

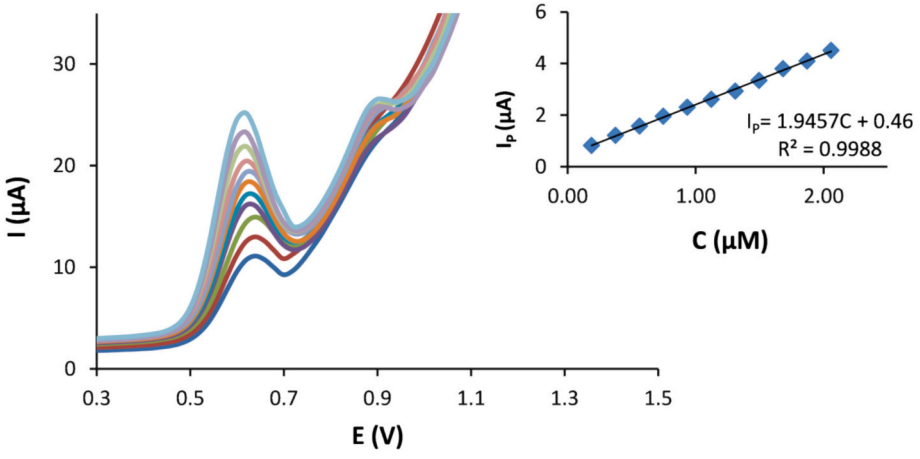

Fig. 4. SWVs corresponding to the calibration of APR in authentic powder within the range 0.19–2.06 μM using 1% MWCNTs/1% CDs/CPE at BRS pH 10.0. Inset: the calibration curve corresponding to the left peak.

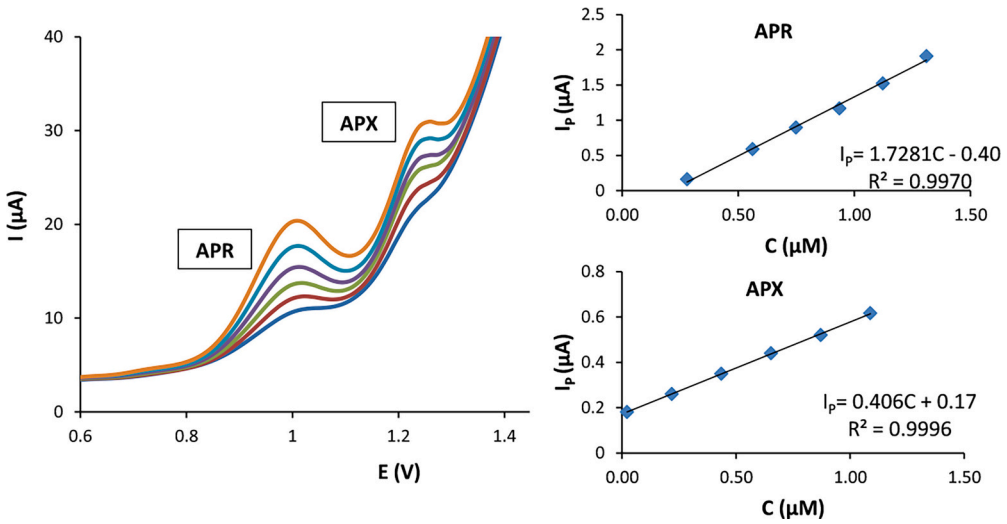

Fig. 5. SWVs corresponding to the simultaneous calibration of APR and APX in spiked plasma within the range 0.28–1.31 µM and 0.02–1.09 µM, respectively, using 2% ZnO/1%CDs/CPE electrode and BRS at pH 4.0. Inset: the calibration curves corresponding to each drug.

Table 2
Regression analysis for simultaneous determination of APR and APX in spiked plasma.

	APR	APX
Working electrode	2% ZnO/1% CDs/CPE	
Linearity range	0.28–1.31 µM (0.15–0.70 µg/mL)	0.02–1.09 µM (0.01–0.50 µg/mL)
Correlation coefficient R2	0.9970	0.9996
Slope	1.7280	0.4060
Intercept	0.40	0.17
LOQ	0.25 µM	0.02 µM
LOD	0.07 µM	0.01 µM

98.36% for APR and from 96.94% to 101.32% for APX, with precision values ranging from 1.91% to 4.12% for APR and from 2.31% to 3.12% for APX (Table 3).

3.8.2.3. Selectivity. Different aliquots from two different lots of human plasma were added to 10 mL BRS pH 4.0. The obtained voltammograms revealed that no interference peaks were observed.

3.8.2.4. Carry-over. The carry-over effect should be investigated to reveal any residuals from highly concentrated samples that would contaminate subsequent samples, especially those with low concentrations, resulting in false results. An unspoked aliquot from human plasma was added to 10 mL BRS pH 4.0 using scratched 2% ZnO/1% CDs /CPE, after measuring a highly concentrated sample. No peak was observed for the unspoked aliquot.

3.8.2.5. Absolute recovery. To ensure that the extraction process is effective, two concentration levels (LQC and HQC) were measured in pre-extraction human plasma (drugs spiked in plasma and then they were extracted) and in post-extraction samples (drugs spiked in plasma after it was extracted). The absolute recovery was measured as the % ratio between the peak current obtained from the spiked plasma to the peak current in the neat solvent. The absolute recoveries of APR were found to be 96.74% with %RSD 3.47 and 97.36% with %RSD 1.36 for LQC and HQC, respectively. The absolute recoveries of APX were found to be 95.37% with %RSD 2.32 and 98.14% with %RSD 2.97 for LQC and HQC, respectively.

3.8.2.6. Matrix effect. The obscure matrix effect from indigenous components in the plasma can be investigated through the analysis of different batches of blank human plasma. Different aliquots were spiked in three different human plasma batches to obtain the LQC and HQC levels; each one was measured in three replicates. The matrix factor (MF) was calculated as the % ratio between the peak current obtained from the spiked plasma to the peak current in the neat solvent. The MF ratios for APR were found to be 97.32 with %RSD 3.12 and 98.36 with % RSD 2.59 for LQC and HQC, respectively. Meanwhile, the MF ratios for APX were found to be 96.36 with %RSD 4.01 and 99.97 with % RSD 3.21 for LQC and HQC, respectively.

3.8.2.7. Stability. The stability study was conducted according to FDA guidelines to simulate the obstacles that are likely to be encountered during the analytical steps. The stability study was performed on LQC and HQC using a freshly prepared stock solution. Each concentration

Table 3
The accuracy and precision data for the determination of APR and APX in spiked human plasma*.

APR					APX				
	Intraday		**Inter-day**			**Intraday**		**Inter-day**	
	%Recovery	%RSD	%Recovery	%RSD		%Recovery	%RSD	%Recovery	%RSD
LLOQ (0.28 µM)	98.41	3.21	97.36	3.97	**LLOQ (0.02 µM)**	97.32	3.32	96.94	2.31
LQC (0.56 µM)	101.31	4.21	97.12	4.12	**LQC (0.06 µM)**	98.36	2.94	101.32	3.12
MQC (0.84 µM)	97.31	2.31	98.32	2.67	**MQC (0.44 µM)**	100.36	1.98	99.63	2.36
HQC (1.12 µM)	97.36	3.67	98.36	1.91	**HQC (0.87 µM)**	99.65	2.01	98.36	2.74

* Each value is an average of six replications.

was measured in six replicates and compared with the nominal one.

3.8.2.8. Bench top stability. The purpose of benchtop stability was to make sure that the analyte concentration and stability were unaffected by the overall amount of time spent preparing plasma samples. The solutions to obtain LQC and HQC levels were stored at room temperature for 6 h. The obtained recoveries were compared to the freshly prepared solutions, which revealed adequate stability (Table 4).

3.8.2.9. Freeze and thaw stability. Different aliquots were spiked in human plasma in three replicates to obtain the LQC and HQC concentration levels. Samples were stored at −80 °C for 12 h, and then they were allowed to thaw at room temperature. The freeze and thaw cycles were repeated three times. The spiked samples showed good stability, as shown in Table 4.

3.8.2.10. Long-term stability. Spiked samples to obtain two concentration levels (LQC and HQC) were stored at −80 °C for around 20 days, which simulates the time between sample withdrawal and analysis. The recoveries obtained after long-term stability conditions showed good stability of the samples (Table 4).

3.8.2.11. Dilution integrity. Spiked plasma solutions were prepared at concentration levels 22.46 and 17.42 μM for APR and APX, respectively, which were diluted by two-fold with blank human plasma to obtain 11.23 and 8.71 μM for APR and APX, respectively. Also, Spiked plasma solutions were prepared at concentration levels 44.92 and 32.68 μM for APR and APX, respectively, which were diluted by fourfold with blank human plasma to obtain 11.23 and 8.71 μM APR and APX, respectively. The LOQ and HQC solutions were obtained upon dilution with 10 mL of BRS at pH 4.0. The accuracy results were 96.54% with %RSD 3.21 and 102.34 with %RSD 2.64 for two and four-fold dilutions of APR. While the accuracy results were 101.74% with %RSD 4.12 and 99.42 with % RSD 1.97 for two and four-fold dilutions of APX.

3.9. Method applications

3.9.1. Determination of APR in capsule dosage form

The proposed method was employed for the determination of APR in capsule dosage form as described under ***sections II.F and II.H***. Three different concentrations were measured, and the obtained results showed acceptable accuracy and precision (**Table S1**).

3.9.2. Simultaneous determination of APR and APX in human plasma

The validated analytical method was implemented for the simultaneous determination of the studied drugs in spiked human plasma following the procedure described in ***sections II.G and II.H***. Acceptable accuracy and precision were obtained as illustrated in **Table S2**.

Table 4
Datasheet for the stability studied under different conditions for the determination of APR and APX in spiked human plasma*.

Studied term	QC levels	APR		APX	
		% Recovery	% RSD	% Recovery	% RSD
Benchtop stability	**LQC**	96.32	3.74	103.36	1.45
	HQC	97.74	2.97	97.17	2.97
Freeze and thaw stability	**LQC**	95.36	4.01	96.14	3.14
	HQC	102.47	2.01	101.46	3.97
Long-term stability	**LQC**	102.36	1.97	100.97	2.76
	HQC	98.43	3.07	98.76	4.01

* Each value is an average of six replicates.

3.10. Evaluation of the greenness of the proposed method

Throughout the synthesis of the working electrodes and the analytical steps, green assessment tools were employed. These matrices aim to promote the development of innovative analytical methods that align with global sustainability goals. The Modified Complementary Green Analytical Procedure Index (ComplexMoGAPI) provides a comprehensive evaluation of the developed method using a color scale ranging from green to yellow to red, indicating low, medium, and high environmental impact, respectively [60–62]. The pictograms represent aspects such as sample collection and preparation, solvents and reagents used in the electrochemical analysis, all instrumentation employed, and the waste generated during the analytical process. The hexagonal section at the bottom of the figure pertains to the steps involved in synthesizing the working electrodes. As shown in Fig. 6a and b, 12 green regions out of 25 were obtained for the method used in the determination of the capsule dosage form, with a scoring system value of 81. Meanwhile, 11 green regions were obtained using the analytical method for the simultaneous determination of APR and APX in human plasma, with a score of 78. These assessments reflect the good sustainability of the developed methods.

The second metric considered is the Blue Applicability Grade Index (BAGI) [63]. This index complements the previous one by focusing on the practicality of the developed method. It also uses a color scale: dark blue, blue, light blue, and white, indicating high, medium, low, and no practicality, respectively. As shown in Fig. 6c and d, the analytical methods successfully support both qualitative and quantitative analysis of APR in capsule dosage forms and the simultaneous determination of APR and APX in human plasma, respectively. The analytical procedures are fast, allowing for the measurement of more than 10 samples per hour, and require only small sample volumes. For the first method, no sample concentration is necessary before analysis. In the proposed method for simultaneous determination in plasma, both APR and APX can be extracted and detected simultaneously at the nanoscale, offering high practicality. The score at the center of the BAGI shape exceeds 60, reflecting the strong practical applicability of the method.

3.11. Comparison with previously developed methods

Table 5 provides a summary of the various voltammetric methods that have been developed for the determination of APR and APX. Compared to existing techniques, our developed method for APR demonstrates a wide linear range, which is particularly advantageous for analyzing samples with varying concentrations and across different electrode materials. Moreover, this method represents the first validated approach for determining APR in capsule dosage forms. The method we established for the simultaneous determination of APR and APX in plasma introduces, for the first time toward precison medicine, to assess potential interactions between the two studied drugs. The two voltammetric methods previously developed for the quantification of APX are not suitable for the simultaneous determination of APR and APX [11,36]. The first method involves measurements at pH 5.0, where the right oxidation peak of APR overlaps and interferes. The second method relies on the oxidation of a redox pair (ferricyanide/ferrocyanide) at the electrode surface. When APX is present, it blocks or interferes with the surface, hindering the redox reaction. The presence of oxidizable APR would also interfere with this system.

4. Conclusion

This study successfully developed and validated voltammetric methods for the simultaneous determination of APR and APX in human plasma, as well as the individual determination of APR in capsule dosage form. By incorporating eco-friendly nanoparticles into carbon paste electrodes, the methods demonstrated high sensitivity, accuracy, and environmental compatibility. Collectively, these findings underscore the

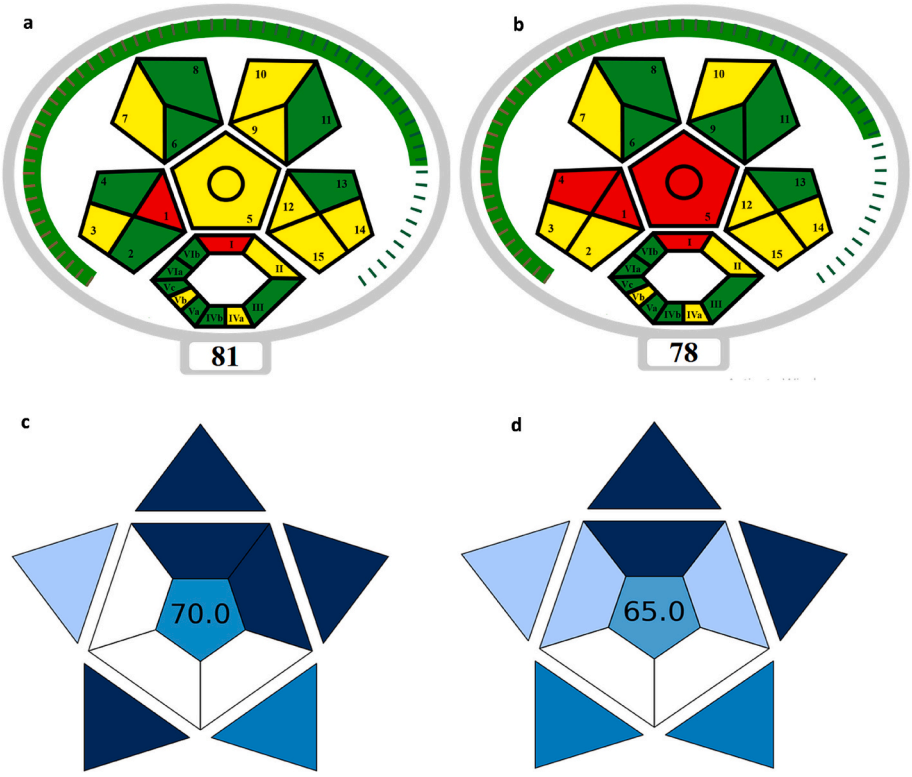

Fig. 6. Green assessment for the determination of APR in capsule dosage forms using ComplexMoGAPI (a) and BAGI (c) tools. Green assessment for the simultaneous determination of APR and APX in human plasma using ComplexMoGAPI (b), BAGI (d) tools. (For interpretation of the references to color in this figure legend, the reader is referred to the web version of this article.)

Table 5
Summary of previously reported voltammetric methods for the determination of APR and APX.

Determined drug	Principle	Working electrode	Linearity range	Limits of detection and quantitation	Application
APR	Oxidation of APR at a modified glassy carbon electrode using phosphate buffer solution at pH 7.0. The I-V response to verified concentration of APR was studied [11]	A glassy carbon electrode modified with synthesized iron oxide nanoparticles was employed	2.20 nM- 4.10 μM	–	–
	Oxidation of APR at a modified carbon paste electrode using BRB at pH 10.0. **(This work)**	Carbon paste electrode modified with zinc oxide nanoparticles and synthesized carbon dots	0.19–2.06 μM	LOD: 0.04 μM LOQ: 0.15 μM	Capsules
APX	Oxidation of APX on the modified carbon paste electrode using phosphate buffer at pH 5 and heptane sulphonic acid as anionic surfactant [35]	Carbon paste electrode modified with multiwall carbon nanotubes.	1.99–107.00 μM	LOD: 0.68 μM LOQ: 1.99 μM	Tablets and a Spiked human sample
	Indirect determination of APX using ferrocyanide at pH 4. The anodic peak current for the redox pair is quantitatively reduced in the presence of APX, depending on the filtering effect of aerogel used in the fabrication of the working electrode [36]	Glassy carbon electrode modified by electrodeposition of synthesized bismuth ferrite nanoparticles and effectively oxidized graphene oxide aerogel.	0.02–21.76 μM	LOQ: 0.02 μM	Human plasma samples
APR and APX	Simultaneous determination of both drugs at a modified carbon paste electrode using BRB at pH 4.0. **(This work)**	Carbon paste electrode modified with multi-wall carbon nanotubes and synthesized carbon dots	For APR: 0.28–1.31 μM For APX: 0.02–1.09 μM	For APR: LOD: 0.07 μM LOQ: 0.25 μM For APX: LOD: 0.01 μM LOQ: 0.02 μM	Human plasma samples

suitability and promising applicability of the developed sensors as a step toward precision medicine platforms for evaluation of potential drug–-drug interactions, as well as for routine quality control laboratories for effective drug level monitoring.

Author contributions statement

All authors conceived and designed the study. D. performed the experiments and collected the data, analyzed and interpreted the results, write the original manuscript. A.B.C.E critically revised the manuscript for important intellectual content. All authors read and approved the final manuscript.

CRediT authorship contribution statement

Rasha Th. El-Eryan: Writing – review & editing, Supervision, Project administration, Investigation, Formal analysis, Conceptualization. **Mona S. Elshahed:** Writing – review & editing, Project administration, Investigation, Formal analysis, Conceptualization. **Dalia Mohamed:** Writing – review & editing, Project administration, Investigation, Formal analysis, Conceptualization. **Azza A. Ashour:** Writing – original draft, Visualization, Validation, Software, Methodology, Investigation, Formal analysis, Conceptualization. **Heba T. Elbalkiny:** Writing – review & editing, Supervision, Project administration, Investigation, Formal analysis, Conceptualization.

Ethics statement

The ethical approval was received from the Scientific Research Ethics Committee at the Faculty of Pharmacy, Helwan University, with reference number (06H2025).

Funding

Tha authors did not receive financial support for the research. The authors will apply for coverage article processing chargea through EKB in accordance with the national publishing agreement.

Declaration of competing interest

The authors declare that they have no known competing financial interests or personal relationships that could have appeared to influence the work reported in this paper.

Appendix A. Supplementary data

Supplementary data to this article can be found online at https://doi.org/10.1016/j.microc.2026.118653.

Data availability

Data will be made available on request.

References

[1] T.M. Dando, C.M. Perry, A review of its use in the prevention of chemotherapy-induced nausea and vomiting, Drugs 64 (2024) 777–792, https://doi.org/10.2165/00003495-200464070-00013.
[2] V.S. Tateosian, K. Champagne, T.J. Gan, What is new in the battle against postoperative nausea and vomiting? Best Pract. Res. Clin. Anaesthesiol. 32 (2018) 137–148, https://doi.org/10.1016/j.bpa.2018.06.005.
[3] W.S. MERCK and CO., INC, Product information, Aprepitant (Emend) (2003) 1–12.
[4] M.S. Aapro, C.M. Walko, Aprepitant: drug-drug interactions in perspective, Ann. Oncol. 21 (2010) 2316–2323, https://doi.org/10.1093/annonc/mdq149.
[5] K.V. Hurst, J.M. O'Callaghan, A. Handa, Quick reference guide to apixaban, Vasc. Health Risk Manag. 13 (2017) 263–267, https://doi.org/10.2147/VHRM.S121944.
[6] S. Halvorsen, D. Atar, H. Yang, R. De Caterina, C. Erol, D. Garcia, C.B. Granger, M. Hanna, C. Held, S. Husted, E.M. Hylek, P. Jansky, R.D. Lopes, W. Ruzyllo, L. Thomas, L. Wallentin, Efficacy and safety of apixaban compared with warfarin according to age for stroke prevention in atrial fibrillation: observations from the ARISTOTLE trial, Eur. Heart J. 35 (2014) 1864–1872, https://doi.org/10.1093/eurheartj/ehu046.
[7] W. Byon, S. Garonzik, R.A. Boyd, C.E. Frost, Apixaban: a clinical pharmacokinetic and Pharmacodynamic review, Clin. Pharmacokinet. 58 (2019) 1265–1279, https://doi.org/10.1007/s40262-019-00775-z.
[8] A. Werońska, A. Undas, E. Wypasek, Reduced-dose apixaban in cancer-associated thrombosis: a single-center experience, Pol. Arch. Intern. Med. 133 (2023) 3–5, https://doi.org/10.20452/pamw.16609.
[9] Bristol-Myers Squib Canada Inc., Product information. Eliquis (apixaban), 2012.
[10] P.H. Shum, L. Dennany, Towards voltammetric point of care detection of leucovorin, Analyst 149 (2024) 2655–2663, https://doi.org/10.1039/d4an00227j.
[11] M.M. Rahman, S.B. Khan, M. Faisal, A.M. Asiri, M.A. Tariq, Detection of aprepitant drug based on low-dimensional un-doped iron oxide nanoparticles prepared by a solution method, Electrochim. Acta 75 (2012) 164–170, https://doi.org/10.1016/j.electacta.2012.04.093.
[12] P. Singh, A. Bali, Derivative spectrophotometric methods for determination of Aprepitant in bulk and pharmaceutical formulation, J. Appl. Spectrosc. 5 (2013) 156–160, https://doi.org/10.1007/s10812-023-01471-4.
[13] E. Souri, A. Abbasi, M. Amanlou, M.B. Tehrani, Spectrophotometric determination of aprepitant in bulk and pharmaceutical dosage forms using bromocresol green as chromogenic reagent, Asian J. Chem. 30 (2018) 1331–1334.
[14] M. Chaitanya, T.H. Kumar, S. Koduru, S. Kalepu, Quantification of aprepitant via charge transfer complexation reactions through visible spectrophotometric methods, J. Appl. Spectrosc. 91 (2025) 1418–1429, https://doi.org/10.1007/s10812-025-01868-3.
[15] S. Nama, B.R. Chandu, B.Z. Awen, M. Khagga, Development and validation of a new RP-HPLC method for the determination of aprepitant in solid dosage forms, Trop. J. Pharm. Res. 10 (2011) 491–497, https://doi.org/10.4314/tjpr.v10i4.15.
[16] S. Ashok, C.V. Raghunadhababu, M. Satish Varma, G. Balaswamy, Separation and quantification of process related impurities and diastereomers in aprepitant bulk drug substance, J. Liq. Chromatogr. Relat. Technol. 35 (2012) 677–687, https://doi.org/10.1080/10826076.2011.606586.
[17] V. Kiran Kumar, N.A. Raju, S. Begum, J.S. Rao, T. Satyanarayana, The estimation of aprepitant in capsules dosage forms by RP-HPLC, Res. J. Pharm. Tech 2 (2009) 1–11. www.rjptonline.org.
[18] S. Nama, B.Z. Awen, B.R. Chandu, M. Khagga, A validated stability indicating RP-HPLC method for the determination of aprepitant in bulk and pharmaceutical dosage forms, recent res, Sci. Technol. 3 (2011) 16–24.
[19] C.M. Chavez-Eng, M.L. Constanzer, B.K. Matuszewski, Simultaneous determination of Aprepitant and two metabolites in human plasma by high-performance liquid chromatography with tandem mass spectrometric detection, J. Pharm. Biomed. Anal. 35 (2004) 1213–1229, https://doi.org/10.1016/j.jpba.2004.03.020.
[20] D. Sharma, V.R. Chauhan, K.B. Vyas, Spectrophotometric determination of apixaban in bulk drug and oral dosage formulation, International Journal of Scientific Research in Science and Technology 6 (2019) 377–385, https://doi.org/10.32628/ijsrst207263.
[21] M.A. Tantawy, N.A. El-Ragehy, N.Y. Hassan, M. Abdelkawy, Stability-indicating spectrophotometric methods for determination of the anticoagulant drug apixaban in the presence of its hydrolytic degradation product, Spectrochim, Acta Part A Mol. Biomol. Spectrosc. 159 (2016) 13–20, https://doi.org/10.1016/j.saa.2016.01.029.
[22] B. Mahendra, Sundari K. Harika, T. Vimalakkannan, Method developed for the determination of apixaban by using UV spectrophotometric, Int. J. Res. Pharm. Chem. Anal. 1 (2019) 83–87, https://doi.org/10.33974/ijrpca.v1i3.115.
[23] A.G. Radhika, A. Singh, A. Sowmya, A.H.M.V. Bakshi, N. Boggula, Comparative studies of apixaban in bulk and its formulations by UV-spectroscopy (zero derivatives and area under curve), Int. J. Pharm. Biol. Sci. 8 (2018) 1002–1008. https://www.researchgate.net/publication/330667197.
[24] K. Anusha, G. Sowjanya, S. Ganapaty, Development and validation of UV spectrophotometric methods for apixaban in tablets, Eur. J. Biomed. Pharm. Sci. 5 (2018) 929–933.
[25] R.I. El-Bagary, E.F. Elkady, N.A. Farid, N.F. Youssef, Validated spectrofluorimetric methods for the determination of apixaban and tirofiban hydrochloride in pharmaceutical formulations, Spectrochim. Acta A Mol. Biomol. Spectrosc. 174 (2017) 326–330, https://doi.org/10.1016/j.saa.2016.11.048.
[26] X. Delavenne, P. Mismetti, T. Basset, Rapid determination of apixaban concentration in human plasma by liquid chromatography/tandem mass spectrometry: application to pharmacokinetic study, J. Pharm. Biomed. Anal. 78–79 (2013) 150–153, https://doi.org/10.1016/j.jpba.2013.02.007.
[27] N. Zheng, L. Yuan, Q.C. Ji, H. Mangus, Y. Song, C. Frost, J. Zeng, A.F. Aubry, M. E. Arnold, "Center punch" and "whole spot" bioanalysis of apixaban in human dried blood spot samples by UHPLC-MS/MS, J. Chromatogr. B anal. Technol. Biomed. Life Sci. 988 (2015) 66–74, https://doi.org/10.1016/j.jchromb.2015.02.023.
[28] S. Lindahl, R. Dyrkorn, O. Spigset, S. Hegstad, Quantification of apixaban, dabigatran, edoxaban, and rivaroxaban in human serum by UHPLC-MS/MS - method development, validation, and application, Ther. Drug Monit. 40 (2018) 369–376, https://doi.org/10.1097/FTD.0000000000000509.
[29] S.B. Landge, S.A. Jadhav, S.B. Dahale, P.V. Solanki, S.R. Bembalkar, V.T. Mathad, Development and validation of stability indicating RP-HPLC method on core shell column for determination of degradation and process related impurities of apixaban—an anticoagulant drug, Am. J. Anal. Chem. 06 (2015) 539–550, https://doi.org/10.4236/ajac.2015.66052.
[30] A. Chitale, P. Hamrapurkar, Development and validation of assay method for estimation of Apixaban in bulk drug and its marketed formulation, Int. J. Adv. Res. Ideas Innov. Technol. 4 (2018) 367–370.
[31] Velusamy B. Subramanian, N.K. Katari, T. Dongala, S.B. Jonnalagadda, Stability-indicating RP-HPLC method development and validation for determination of nine impurities in apixaban tablet dosage forms. Robustness study by quality by design approach Velusamy, Biomed. Chromatogr. 34 (2019) 1–8, https://doi.org/10.1002/bmc.4719.
[32] F. Gouveia, J. Bicker, J. Santos, M. Rocha, G. Alves, A. Falcão, A. Fortuna, Development, validation and application of a new HPLC-DAD method for simultaneous quantification of apixaban, dabigatran, edoxaban and rivaroxaban in human plasma, J. Pharm. Biomed. Anal. 181 (2020) 1–8, https://doi.org/10.1016/j.jpba.2020.113109.
[33] I. Al-Ani, M. Hamad, R. Al-Shdefat, K. Mansoor, F. Gligor, W.A. Dayyih, Development and validation of a stability indicating RP-HPLC method of apixaban in commercial dosage form, Int. J. Pharm. Sci. Res. 12 (2021) 241–251, https://doi.org/10.13040/IJPSR.0975-8232.12(1).241-51.

[34] A. Demir, A. Bulduk, H. Enginar, C. Çifci, A green HPLC method for the determination of apixaban in pharmaceutical products: development and validation, Rev. Anal. Chem. 42 (2023) 1–28, https://doi.org/10.1556/1326.2023.01155.
[35] M. Rizk, M.A. Sultan, E.A. Taha, A.K. Attia, Y.M. Abdallah, Sensitive validated voltammetric determination of apixaban using a multi-walled carbon nanotube-modified carbon paste electrode: application to a drug product and biological sample, Anal. Methods 9 (2017) 2523–2534, https://doi.org/10.1039/C7AY00244K.
[36] P. Shahbazi-Derakhshi, M. Abbasi, A. Akbarzadeh, A. Mokhtarzadeh, H. Hosseinpour, J. Soleymani, A ratiometric electrochemical probe for the quantification of apixaban in unprocessed plasma samples using carbon aerogel/BFO modified glassy carbon electrodes, RSC Adv. 13 (2023) 21432–21440, https://doi.org/10.1039/d3ra03293k.
[37] A.S. Farag, Voltammetric determination of acetaminophen in pharmaceutical preparations and human urine using glassy carbon paste electrode modified with reduced graphene oxide, Anal. Sci. 38 (2022) 1213–1220, https://doi.org/10.1007/s44211-022-00150-2.
[38] R. de O. Silva, É.A. da Silva, A.R. Fiorucci, V.S. Ferreira, Electrochemically activated multi-walled carbon nanotubes modified screen-printed electrode for voltammetric determination of sulfentrazone, J. Electroanal. Chem. 835 (2019) 220–226, https://doi.org/10.1016/j.jelechem.2019.01.018.
[39] M. Shah, P. Kolhe, S. Gandhi, Nano-assembly of multiwalled carbon nanotubes for sensitive voltammetric responses for the determination of residual levels of endosulfan, Chemosphere 321 (2023) 1–9, https://doi.org/10.1016/j.chemosphere.2023.138148.
[40] M. Defrise, P. Grangeat, A low-cost voltammetric sensor based on multi-walled carbon nanotubes for highly sensitive and accurate determination of nanomolar levels of the anticancer drug Ribociclib in bulk and biological fluids, Anal. Methods 16 (2024) 1623–1630, https://doi.org/10.1002/9780470611784.ch2.
[41] A.S. Agnihotri, A. Varghese, M. Nidhin, Transition metal oxides in electrochemical and bio sensing: a state-of-art review, Appl. Surf. Sci. Adv. 4 (2021) 100072, https://doi.org/10.1016/j.apsadv.2021.100072.
[42] K.M. Omer, D.I. Tofiq, A.Q. Hassan, Solvothermal synthesis of phosphorus and nitrogen doped carbon quantum dots as a fluorescent probe for iron(III), Microchim. Acta 185 (2018), https://doi.org/10.1007/s00604-018-3002-4.
[43] V. Bressi, I. Chiarotto, A. Ferlazzo, C. Celesti, C. Michenzi, T. Len, D. Iannazzo, G. Neri, C. Espro, Voltammetric sensor based on waste-derived carbon Nanodots for enhanced detection of nitrobenzene, ChemElectroChem 10 (2023), https://doi.org/10.1002/celc.202300004.
[44] The United States Pharmacopeia and National Formulary :The Official Compendia of Standards, Asian Edition, USP 39-NF34, the United States Pharmacopeial Conversion Inc., Rockvill, MD, 2016.
[45] R.T. El-Eryan, M.S. Elshahed, D. Mohamed, A.A. Ashour, H.T. Elbalkiny, Functionalized novel carbon dots from bell pepper seeds for sustainable green edoxaban quantification, BMC Chem. 19 (2025), https://doi.org/10.1186/s13065-025-01427-z.
[46] Th. Rasha, S.S. Toubar El-Eryan, Azza A. Ashour, M.S. Elshahed, Zirconium oxide nanoparticles modified carbon paste electrode for simultaneous voltammetric determination of mebendazole and levamisole hydrochloride in pharmaceutical formulation and human plasma, Electroanalysis 34 (2022) 1–14, https://doi.org/10.1002/elan.202100559.
[47] R. El-Eryan, S.S. Toubar, A.A. Ashour, M.S. Elshahed, Application of analytical eco-scale and complex-GAPI tools for green assessment of a new simple nanoparticle modified carbon paste electrode method for voltammetric determination of mosapride citrate in pharmaceutical dosage form and human plasma, Microchem. J. 178 (2022) 1–8, https://doi.org/10.1016/j.microc.2022.107347.
[48] K. Ngamchuea, B. Tharat, P. Hirunsit, S. Suthirakun, Electrochemical oxidation of resorcinol: mechanistic insights from experimental and computational studies, RSC Adv. 10 (2020) 28454–28463, https://doi.org/10.1039/d0ra06111e.
[49] D.A. Skoog, D. West, F.J. Holler, Mary Finch, Fundamentals of Analytical Chemistry, 9th ed., Philadelphia, Estados Unidos, 2013.
[50] H. Xing, L. Wu, X. Li, Zn/N co-doped TiO2 nanotubes for enhancement of photocatalytic degradation of pentachlorophenol, Int. J. Electrochem. Sci. 17 (2022) 1–10, https://doi.org/10.20964/2022.06.32.
[51] E. Laviron, Electroanal. Chem., in: 1st ed., Journal of Electroanalytical Chemistry and Interfacial Electrochemistry, Netherlands, 1979, pp. 19–28.
[52] F. Varmaghani, V. Nemati, Mechanistic aspects of electro-oxidative generated triazolinediones in the presence of amines-EC' versus ECE mechanism, J. Electroanal. Chem. 918 (2022) 116447, https://doi.org/10.1016/j.jelechem.2022.116447.
[53] E.L. Dolengovski, T.V. Gryaznova, O.G. Sinyashin, E.L. Gavrilova, K.V. Kholin, Y. H. Budnikova, Morpholine radical in the electrochemical reaction with quinoline N-oxide, Catalysts 13 (2023) 1–15, https://doi.org/10.3390/catal13091279.
[54] J.Y. Becker, Anodic oxidation of aliphatic and aromatic amides, bisamides and related derivatives, ChemElectroChem 11 (2024) 1–17, https://doi.org/10.1002/celc.202400023.
[55] B. List, R.A. Lerner, C.F. Barbas, Proline-catalyzed direct asymmetric aldol reactions, J. Am. Chem. Soc. 122 (2000) 2395–2396, https://doi.org/10.1021/ja994280y.
[56] S.P. Kounaves, Voltammetric Techniques, Oxford University Press, Oxford, UK, 1997.
[57] B.R. Eggins, Chemical Sensors and Biosensors, 2nd ed., John Wiley & Sons, west sussex, england, 2008.
[58] I.C.H. Guideline, Validation of analytical procedures: Text and methodology Q2 (R1), in: Int. Conf. Harmon, Geneva, Switz, 2013, https://doi.org/10.1002/9781118532331.ch23.
[59] US Food and Drug Administration, 2013.
[60] F.R. Mansour, K.M. Omer, J. Płotka-Wasylka, A total scoring system and software for complex modified GAPI (ComplexMoGAPI) application in the assessment of method greenness, green, Anal. Chem. 10 (2024) 1–4, https://doi.org/10.1016/j.greeac.2024.100126.
[61] J. Płotka-Wasylka, W. Wojnowski, Complementary green analytical procedure index (ComplexGAPI) and software, Green Chem. 23 (2021) 8657–8665, https://doi.org/10.1039/D1GC02318G.
[62] J. Płotka-Wasylka, A new tool for the evaluation of the analytical procedure: green analytical procedure index, Talanta 181 (2018) 204–209, https://doi.org/10.1016/j.talanta.2018.01.013.
[63] N. Manousi, W. Wojnowski, J. Płotka-Wasylka, V. Samanidou, Blue applicability grade index (BAGI) and software: a new tool for the evaluation of method practicality, Green Chem. 25 (2023) 7598–7604, https://doi.org/10.1039/d3gc02347h.